The Astrophysical Journal, 954:79 (15pp), 2023 September 1 https://doi.org/10.3847/1538-4357/ace627

Speed and Acceleration of Coronal Mass Ejections Associated with Sustained Gamma-Ray Emission Events Observed by Fermi/LAT

Pertti Mäkelä[1,2], Nat Gopalswamy[2], Sachiko Akiyama[1,2], Hong Xie[1,2], and Seiji Yashiro[1,2]
[1] The Catholic University of America, 620 Michigan Avenue, N.E. Washington, DC 20064, USA; pertti.makela@nasa.gov, makela@cua.edu
[2] NASA Goddard Space Flight Center, 8800 Greenbelt Road, Greenbelt, MD 20771, USA
Received 2023 March 20; revised 2023 June 30; accepted 2023 July 9; published 2023 August 24

Abstract

The sustained gamma-ray emission (SGRE) from the Sun is a prolonged enhancement of >100 MeV gamma-ray emission that extends beyond the flare impulsive phase. The origin of the >300 MeV protons resulting in SGRE is debated, with both flares and shocks driven by coronal mass ejections (CMEs) being the suggested sites of proton acceleration. We compared the near-Sun acceleration and space speed of CMEs with "Prompt" and "Delayed" (SGRE) gamma-ray components. We found that "Delayed"-component-associated CMEs have higher initial accelerations and space speeds than "Prompt Only"-component-associated CMEs. We selected halo CMEs (HCMEs) associated with type II radio bursts (shock-driving HCMEs) and compared the average acceleration and space speed between HCME populations with or without SGRE events, major solar energetic particle (SEP) events, metric, or decameter-hectometric (DH) type II radio bursts. We found that the SGRE-producing HCMEs associated with a DH type II radio burst and/or a major SEP event have higher space speeds and especially initial accelerations than those without an SGRE event. We estimated the radial distances and speeds of the CME-driven shocks at the end time of the 2012 January 23 and March 7 SGRE events using white-light images of STEREO Heliospheric Imagers and radio dynamic spectra of Wind WAVES. The shocks were at the radial distances of 0.6–0.8 au and their speeds were high enough (≈975 km s^{-1} and ≈750 km s^{-1}, respectively) for high-energy particle acceleration. Therefore, we conclude that our findings support the CME-driven shock as the source of >300 MeV protons.

Unified Astronomy Thesaurus concepts: Solar gamma-ray emission (1497); Solar coronal mass ejections (310); Solar energetic particles (1491)

1. Introduction

The sustained gamma-ray emission (SGRE) from the Sun is a prolonged enhancement of >100 MeV gamma-ray emission that extends beyond the flare impulsive phase. SGRE typically lasts for several hours, extending well beyond the end of the associated soft X-ray flare emission. The first SGRE event at energies above 100 MeV was detected on 1991 June 15 by the Gamma-1 telescope on board the Gamma spacecraft, and it lasted at least 2.16 hr (Akimov et al. 1991). A similar observation of a long-duration >50 MeV gamma-ray emission was reported by Kanbach et al. (1993) during the 1991 June 11 flare. SGREs >100 MeV are produced by >300 MeV protons precipitating from the solar corona into the solar chromosphere, where their interactions with the dense plasma layers create pions, which then decay into the observed >100 MeV gamma rays (e.g., Murphy et al. 1987). The dominant source of >100 MeV gamma rays is neutral pion decay (e.g., Kafexhiu et al. 2018; Gopalswamy 2020). Forrest et al. (1985) first reported a clear detection of >40 MeV gamma rays that require pion production during the extended phase of the 1982 June 3 gamma-ray flare. SGRE events were originally called long-duration gamma-ray flares (LDGRFs; e.g., Ryan 2000). Nowadays they are also known as late-phase >100 MeV gamma-ray emission (LPGRE; e.g., Share et al. 2018) events. A review of gamma-ray observations analogous to Gamma-1 measurements by Ryan (2000) listed 13 LDGRFs between 1982 and 1991. A few more early events have been discovered from observations by nondedicated gamma-ray telescopes (Kuznetsov et al. 2014). Most recently, observations by the Large Area Telescope (LAT; Atwood et al. 2009) on board the Fermi satellite have shown that SGRE events are relatively common (Ackermann et al. 2014; Ajello et al. 2014; Pesce-Rollins et al. 2015; Ackermann et al. 2017; Allafort 2018; Share et al. 2018; Ajello et al. 2021). The >100 MeV SGRE event on 2012 March 7 was observed to last over 20 hr (e.g., Gopalswamy et al. 2018; Share et al. 2018).

The origin of the >300 MeV protons producing SGRE is still debated. Murphy et al. (1987) studied the 1982 June 3 event and suggested a two-phase particle acceleration scenario, where a short-duration impulsive-phase acceleration is followed by a second acceleration phase, probably due to protons accelerated by coronal shocks and resulting in SGREs (see also, Ramaty et al. 1987). Ryan & Lee (1991) investigated the same 1983 June 3 gamma-ray flare and found a good agreement between their model of turbulent solar flare loops and the observed gamma-ray light curves, including the extended emission phase, which their model explained to be due to delayed protons diffusing both in momentum space and spatially in the flare loops. The flare loop scenario requires that flare-accelerated protons must remain trapped and/or be continuously re-accelerated in the coronal loops long after the X-ray flare itself has ended. However, trapping high-energy protons in coronal loops for several hours requires force-free loops (Lau et al. 1993) with a sufficiently low density and turbulence level (Ryan 2000). As an alternative to particle trapping in the coronal loops, Kocharov et al. (1994) suggested a continuous stochastic acceleration due to additional pulses of energy that could

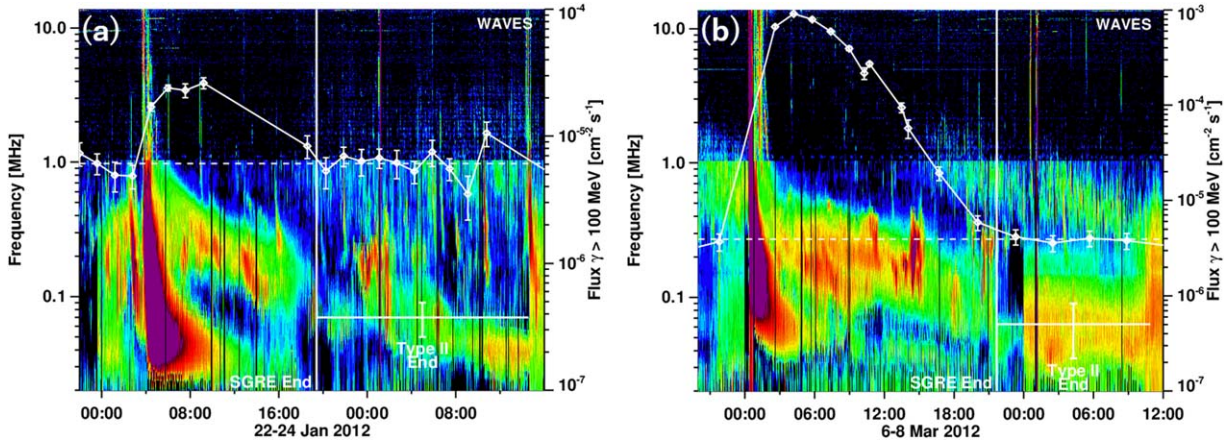

Figure 1. Data points of Fermi/LAT >100 MeV gamma-ray flux overplotted on Wind/WAVES radio dynamic spectra for the 2012 January 23 and March 7 SGRE events. The LAT data points are connected by straight lines to guide the eye. The estimated end times of the SGRE events and type II radio bursts are marked by long and short vertical lines.

explain gamma-ray observations during the extended phase of the 1991 June 15 LDGRF (see also, Akimov et al. 1991, 1996).

Gamma-ray-line observations of the behind-the-limb flare on 1989 September 29 were interpreted to require a spatially extended gamma-ray source and hence to suggest shocks driven by fast and wide coronal mass ejections (CMEs) as a likely source of the gamma-ray-emission-producing particles (e.g., Cliver et al. 1993; Vestrand & Forrest 1993). Recent LAT observations of SGRE events during eruptions occurring behind the solar limb have confirmed that an extended source of gamma rays must exist at the Sun (e.g., Pesce-Rollins et al. 2015; Plotnikov et al. 2017). The CME-driven shock naturally extends over large regions of solar surface allowing the shock-accelerated protons to have access to areas far from the behind-the-limb eruption site. Gopalswamy et al. (2020) forward modeled the CME flux rope and the surrounding shock in the 2014 September 1 behind-the-limb event and found that the Fermi/LAT SGRE source was located far from the flare site —in the space between the flux rope and shock confirming the extended nature of the emission. Hudson (2018) suggested another scenario where closed magnetic loops extended up to the height of several solar radii will capture high-energy protons that might be accelerated by a CME shock and subsequently the loops retract and enable sufficiently large numbers of >300 MeV protons to interact with the solar atmosphere.

Recently, de Nolfo et al. (2019) compared the estimated fluxes of gamma-ray-producing particles precipitating into the solar atmosphere with the fluxes of SEPs escaping into interplanetary space and did not find a significant correlation. They suggested that the lack of correlation rules out the CME-driven shock as a common source of both fluxes. However, Gopalswamy et al. (2021) pointed out that the correlation is high when systematic effects are corrected differently. Kouloumvakos et al. (2020) compared the SGRE time profile observed during the ground-level enhancement (GLE) on 2017 September 10 with the time profiles of simulated shock parameters and found a good match between them, supporting the CME shock as a common source of SGRE-producing protons at the Sun and GLE protons at 1 au. Winter et al. (2018) studied the properties of flares and CMEs with and without SGREs. They found that SGRE events are associated with intense X-class flares but only one-third of the X-class solar flares Fermi/LAT observed have an SGRE event. They also note that fast and wide CMEs are associated with SGRE events. Therefore, their results on the flare and CME associations favor CME-driven shock as the source of >300 MeV protons.

Additional support for the CME-shock scenario is provided by the correlation of the SGRE durations with the durations and the end frequencies of type II radio bursts (Gopalswamy et al. 2018, 2019). Figure 1 shows two examples of concurrent SGRE events and type II radio bursts during the SGRE event in January and March 2012. Although type II radio bursts are produced by CME-shock-accelerated electrons, they indicate the presence of a strong shock that could also accelerate protons to high energies. Therefore, the correlations suggest that CME-driven shocks could be the source of both the electrons resulting in the decameter-hectometric (DH) type II radio bursts and the >300 MeV protons generating the SGRE events. Pesce-Rollins et al. (2022) investigated the EUV wave connection to the behind-the-limb (BTL) flare at S20E140 on 2021 July 17. They found that the time when the EUV wave crosses the limb onto the visible disk and the onset of the LAT >100 MeV flux enhancement are concurrent. They also found a coupling between the peak times of the time derivative of the EUV wave intensity profile observed at 193 Å and the >100 MeV gamma-ray flux suggesting that the EUV wave and the acceleration of the SGRE-producing protons are connected. They found the correlation to be valid in three other Fermi/LAT BTL flares. Pesce-Rollins et al. (2022) conclude that the correlation between the derivative of the EUV wave intensity and gamma-ray flux and the near-simultaneous appearance of a complex type II radio burst indicate that radio, EUV, and gamma-ray emissions share the same source (CME shock) although the emissions originate at different heights in the corona.

The back-precipitation of shock-accelerated protons has been studied using numerical simulations but results so far have not been accordant with one another. Hutchinson et al. (2022) modeled particle precipitation including enhanced turbulence and found scattering to increase back-precipitation but even that being the case the fraction of protons able to precipitate down to the radial distance of 1 $R_\odot$ relative to the injected back-propagating protons is less than 1%. The precipitation fraction decreases as a function of the radial distance of the CME shock. Therefore, they conclude that the CME-driven shocks cannot provide a sufficient flux of >300 MeV protons to explain the SGRE events. Opposite conclusions in support of a CME shock

as the source of the gamma-ray-producing protons have been obtained by Jin et al. (2018) who studied the Fermi behind-the-limb flare on 2014 September 1. Their simulations of the CME-driven shock indicated that the quasi-perpendicular part of the shock had a magnetic connection to the gamma-ray source at the front-side of the Sun and the shock compression ratio increase matched the increase in the observed gamma-ray emission. Afanasiev et al. (2018) simulated proton acceleration in the CME-driven shocks during the 2012 January 23 and May 17 SGRE events. The 2012 May 17 SGRE event was also observed as a GLE by neutron monitors. They concluded that proton acceleration by coronal shocks and diffusive downstream particle transport could explain the SGRE events. However, the authors of the abovementioned studies suggest that more elaborated MHD models for the particle transport back to the Sun are required because of the complex structure of the magnetic fields near the Sun, which the current simulation efforts cannot fully replicate. The lack of direct observations of the precipitating protons close to the Sun leaves the question of whether they can propagate back to the solar atmosphere deep enough open.

The initial acceleration and speed of the CME in part control the formation height and strength of the shock, which in turn affect the particle acceleration efficiency of the shock. Therefore, the CME acceleration and speed provide a proxy for the effectiveness of high-energy particle acceleration in CME-driven shocks. Gopalswamy et al. (2022a) studied SGRE association with on-disk CMEs producing major SEP events and HCMEs with sky-speeds $\geqslant$1800 km s^{-1} during cycle 24. They investigated the initial acceleration and space speed of the CMEs, which they defined to be the instantaneous peak space speed and acceleration obtained from forward fitting of the graduated cylindrical shell (GCS) flux rope model (Thernisien et al. 2009; Thernisien 2011) to the EUV and coronagraph images of the CMEs. They found that the peak space speed and peak initial acceleration of the SGRE-producing CME are 2516 km s^{-1} and 3.87 km s^{-2}, respectively. Gopalswamy et al. (2022a) suggest that the close connection they found between CME kinematics and the SGRE events supports the CME-shock scenario.

In addition to SEP events, type II radio bursts are related to particle acceleration by CME-driven shocks. In this report, we estimate the initial acceleration and space speed of the CMEs associated with the Fermi/LAT solar flares (FLSFs) during solar cycle 24 listed by Ajello et al. (2021). In order to evaluate the feasibility of the CME-driven shocks in producing SGRE events, we compare the average initial acceleration and space speed of CME populations associated with SGRE and SEP events and type II radio bursts. We use space speeds obtained by applying a geometrical correction to close-to-the-limb CMEs or by applying the model by Xie et al. (2004) to HCMEs. Initial acceleration is estimated by assuming that the CME obtains its estimated space speed during the interval extending from the onset time to the peak time of the associated soft X-ray flare (Gopalswamy et al. 2012; Mäkelä et al. 2015). In addition, we estimate the radial distance and the space speed of shocks at the end time of the two longest-duration SGRE events on 2012 January 23 and March 7.

2. Data

In the analysis, we use the catalog published by Ajello et al. (2021) that contains 45 FLSFs with >30 MeV gamma-ray emission in the period 2010 January–2018 January. We do not repeat here all the details of the event data analysis, which are given in Ajello et al. (2021). We briefly describe their categorization method of FLSFs. Ajello et al. (2021) characterized the light curves of the FLSFs based on the associated hard X-ray (HXR) observations made by the Fermi Gamma-ray Burst Monitor (GBM, Meegan et al. 2009). If the early evolution of the gamma-ray emission was synchronous with the Fermi/GBM HXR evolution, the flare was deemed to have an impulsive "Prompt" component lasting $\lesssim$10 minutes. If the flare had a second phase of gamma-ray emission without a corresponding HXR evolution, the flare was deemed to have a gradual "Delayed" component that could last up to $\approx$20 hr. Ajello et al. (2021) found that a total of 39 out of the 45 FLSFs had detectable levels of >100 MeV emission. One should note that Fermi/LAT does not observe the Sun continuously, the average LAT measurement interval lasts about 30 minutes (Ajello et al. 2021). Of those 45 FLSFs, they classified 6 flares as "Prompt Only" and 4 flares as "Delayed only". In 10 flares both the "Prompt" and "Delayed" emissions were detected by LAT and 6 flares were detected with LAT Low Energy (LLE) analysis only.

The existence of the DH type II radio bursts is based on Wind spacecraft's radio and plasma wave instrument (WAVES, Bougeret et al. 1995) observations,[3] STEREO/WAVES instrument (Bougeret et al. 2008) observations, and on the analysis by Gopalswamy et al. 2018, 2019. The metric type II radio burst and soft X-ray flare observations are obtained from the NOAA Solar and Geophysical Event Reports. We adjusted the NOAA-reported flare onset times in some events after inspecting concurrent EUV images and soft X-ray curves of the solar eruption. The CME data near the Sun is provided by the Large Angle and Spectrometric Coronagraph (LASCO, Brueckner et al. 1995) on the Solar and Heliospheric Observatory (SOHO, Domingo et al. 1995) spacecraft. The CME data is collected from the SOHO/LASCO CME Catalogs.[4] SEP event data are from the Major SEP Event list[5] and from the GOES-equivalent >10 MeV intensities calculated using data provided by the High Energy Telescope (HET; von Rosenvinge et al. 2008) on board STEREO. For the shock distance estimation at the end of the SGRE event, we used white-light images of the Sun–Earth Connection Coronal and Heliospheric Investigation (SECCHI, Howard et al. 2008) Heliospheric Imagers (HIs, Eyles et al. 2009) on board the Solar Terrestrial Relations Observatory (STEREO, Driesman et al. 2008) spacecraft. The HI images were provided by the STEREO Archive maintained by the UK Solar System Data Centre.[6] To identify the associated CMEs, we inspected the CME catalogs provided by the Heliospheric Cataloguing, Analysis, and Techniques Service (HELCATS).[7]

3. Estimation Method of the CME Initial Acceleration

The initial acceleration of the CME near the Sun is difficult to measure because the cadence of white-light coronagraphs is limited. In our study we follow the method previously used by

[3] https://cdaw.gsfc.nasa.gov/CME_list/radio/waves_type2.html
[4] https://cdaw.gsfc.nasa.gov/CME_list/index.html, https://cdaw.gsfc.nasa.gov/CME_list/halo/halo.html
[5] https://cdaw.gsfc.nasa.gov/CME_list/sepe/
[6] https://www.ukssdc.ac.uk/solar/stereo/data.html
[7] https://www.helcats-fp7.eu/

Table 1
Initial Acceleration and Space Speed of CMEs Associated with LAT Gamma-ray Flares

Quantity	Main Types		Subtypes of "All Delayed"		
	Prompt Only	All Delayed	Delayed	Prompt Delayed	No-prompt Delayed
(1)	(2)	(3)	(4)	(5)	(6)
Count	6	32	18	8	4
Mean Acceleration (km s^{-2})	1.37	1.75	1.73	1.87	1.62
Mean Space Speed (km s^{-1})	775	1708	1745	1753	1663

Gopalswamy et al. (2012) and Mäkelä et al. (2015). We assume that the CME accelerates from rest to its final maximum speed, which it reaches at the peak time of the associated soft X-ray flare. Zhang & Dere (2006) have shown that the main acceleration phase of the CME coincides with the impulsive phase of the associated X-ray flare. Therefore, we calculate the initial acceleration a of the CME with a formula: $a = V_{\rm Space}/(t_{\rm FlarePeak} - t_{\rm FlareOnset})$, where $V_{\rm Space}$ is the estimated space speed of the CME and $t_{\rm FlarePeak}$ and $t_{\rm FlareOnset}$ are the flare peak and onset times, respectively. The space speed of halo CMEs (HCMEs) has been estimated by using a cone model for HCMEs (Xie et al. 2004) and the space speeds are listed in the SOHO/LASCO HALO CME catalog.[8] For non-HCMEs, the space speed, $V_{\rm Space}$, is calculated from the measured CME speed on the sky plane, $V_{\rm Sky}$, by using a geometrical correction $V_{\rm Sky}/\cos\theta$, where θ is the angle the CME propagation direction makes away from the sky plane. The angle θ depends on the longitude of the flare location. To avoid unrealistically large corrections, we have included in the analysis only non-HCMEs for which θ is $\leqslant 30°$ as seen either from the SOHO or STEREO spacecraft. The method calculates an average over the acceleration phase of the CME. The peak initial acceleration of the CME can be higher than the obtained average initial acceleration as was shown by Gopalswamy et al. (2021).

In general, we know that the CME speed profiles near the Sun vary from event to event and CME speed is an important parameter governing particle acceleration efficiency of the CME-driven shocks. Gopalswamy et al. (2016, 2017) showed that CMEs associated with major SEP events have a hierarchical relationship between the initial acceleration and speed of the CME and the SEP fluence spectral indices (see also, Mäkelä et al. 2019): CMEs associated with filament eruptions have low initial speeds and acceleration and produce the softest SEP spectra at 1 au, while the CMEs with highest initial speed and acceleration have the hardest SEP spectra. The CMEs with an intermediate speed and acceleration result in moderately hard SEP spectra at 1 au. Therefore, initial acceleration and speed provide a proxy for the effectiveness of high-energy particle acceleration in the CME-driven shocks.

3.1. Initial Acceleration and Space Speed of CMEs Associated with LAT Gamma-ray Flares

In our analysis, we use the on-disk gamma-ray events listed in Ajello et al. (2021). Their list contains 45 gamma-ray flares during cycle 24. Ajello et al. (2021) categorized the flares based on whether the "Prompt" or "Delayed" component (SGRE event) of gamma-ray emission was detected. In the 6 events of the 45 events, only "Prompt" (impulsive) emission was detected, 4 events had no detected "Prompt" emission at all, 10 events had both "Prompt" and "Delayed" emissions and the remaining 25 had "Delayed" emission, but the presence of "Prompt" emission could not be excluded because of LAT was not pointing to the Sun at the appropriate time. 32 of the flares were associated with an HCME, 10 were associated with non-HCMEs, and 3 had no associated CME. Based on our own estimations, we changed the CME of the 2014 September 10 flare to the 08:00 UT HCME. We have excluded the three back sided flares, the three flares without CMEs, and the 2017 September 06 X2.2 flare for which we could not estimate the space speed of the CME at 09:48 UT because there is no suitable side view either from SOHO or STEREO-A.

Table 1 lists the total number and the average value of the initial acceleration and space speed of CMEs in different categories. First, we divided the CMEs into two main categories: those associated with flares showing only a "Prompt" component, labeled as "Prompt Only" and those with a "Delayed" component, labeled "All Delayed" in Table 1. The "Prompt Only" flares are impulsive gamma-ray flares and the "All Delayed" ones are SGRE events. Clearly, the impulsive gamma-ray flares are associated with significantly slower CMEs (775 km s^{-1}) than flares with an SGRE event (1708 km s^{-1}). The difference in the initial acceleration is not as clear, but again the CMEs with SGRE events show a larger initial acceleration than those without an SGRE event. From SEP event comparisons by Gopalswamy et al. (2016; see also Mäkelä et al. 2019) we know that higher acceleration and speed indicate that the CME-driven shock produces harder energy spectra, i.e., more likely to have >300 MeV protons. Similar high initial acceleration and fast speed characteristics are shared by CMEs associated with GLEs, which are guaranteed to have >300 MeV protons.

Then we divided the "All Delayed" CMEs into three subcategories: the "Prompt Delayed" CMEs are associated with gamma-ray flares having both emission components, the "No-Prompt Delayed" CMEs do not have a detectable "Prompt" component and the "Delayed" CMEs have a "Delayed" component but the existence of the "Prompt" component is uncertain because of the lack of LAT observations during the impulsive phase of the flare. Differences are now less significant (the sample sizes also become small), but the "Prompt Delayed" CMEs appear to have the highest average initial acceleration and space speed, and the "No-prompt Delayed" CMEs have the lowest ones among the three groups. Most likely the CMEs without associated "Prompt" gamma-ray components are more slowly accelerating CMEs but are still able to produce >300 MeV protons as their space speed becomes high enough in the later phase. Again, similar slower initial acceleration but high later-phase speed has been detected for CMEs producing major SEP events (Gopalswamy et al. 2016). Table A1 in the Appendix lists the data for events included in calculations of Table 1.

[8] https://cdaw.gsfc.nasa.gov/CME_list/halo/halo.html

Table 2
Initial Acceleration and Space Speed of Cycle 24 HCMEs with Metric Type II Radio Bursts

HCME Category	"Delayed" Component (SGRE Event)			No "Delayed" Component		
	Count	Mean Acceleration (km s^{-2})	Mean Space Speed (km s^{-1})	Count	Mean Acceleration (km s^{-2})	Mean Space Speed (km s^{-1})
(1)	(2)	(3)	(4)	(5)	(6)	(7)
DH Type II	23	1.85	1869	37	1.09	1211
No DH Type II	1	Too low statistics		26	1.11	959
SEP Event	17	1.83	2004	13	1.15	1499
SEP Event (w/STEREO)	21	1.70	1858	18	1.07	1396
No SEP Event	7	1.81	1360	50	1.09	1006
No SEP Event (w/STEREO)	3	2.68	1524	45	1.11	992

Table 3
Initial Acceleration and Space Speed of Cycle 24 HCMEs with DH Type II Radio Bursts only

HCME Category	"Delayed" Component (SGRE Event)			No "Delayed" Component		
	Count	Mean Acceleration (km s^{-2})	Mean Space Speed (km s^{-1})	Count	Mean Acceleration (km s^{-2})	Mean Space Speed (km s^{-1})
(1)	(2)	(3)	(4)	(5)	(6)	(7)
SEP Event	1	Too low statistics		3	0.46	1263
SEP Event (w/STEREO)	2	Too low statistics		4	0.38	1265
No SEP Event	3	1.00	1579	13	0.44	1164
No SEP Event (w/STEREO)	2	Too low statistics		12	0.47	1155

4. Comparison with HCMEs Associated with Type II Radio Bursts and Major SEP Events

Because the "All Delayed" gamma-ray flares are mainly associated with HCMEs, we compare their initial acceleration and space speed with HCMEs associated with type II radio bursts and major SEP events. Major SEP events are defined as those with the peak proton flux in the GOES >10 MeV integral channel above 10 particles cm^{-2} s^{-1} sr^{-1}. As SEPs are charged particles, they spiral along the interplanetary magnetic field lines as they propagate away from the acceleration source. Therefore, at Earth we can detect mostly SEP events originating from eruptions occurring in the western hemisphere of the Sun. Some very intense eruptions from the eastern limb can produce particle events at Earth but in that case only at the lower energies.

In general, DH type II radio bursts are well correlated with major SEP events (Gopalswamy et al. 2002; Cliver et al. 2004; Gopalswamy et al. 2019). Both radio and gamma-ray emissions can be detected from all on-disk eruptions because electromagnetic emission can propagate away from the Sun without being significantly affected by coronal or interplanetary medium. Type II solar radio bursts occur at the fundamental and second harmonic of local plasma frequency that depends on the electron density upstream of the CME shock. Because the electron number density decreases as a function of the radial distance, the plasma frequency decreases away from the Sun and higher frequency emissions originating from a lower height can propagate freely outwards. Therefore, the type II burst can be identified in the radio dynamic spectra as an intensity feature slowly drifting toward lower frequencies at a rate that depends on the shock speed and the density scale height of the ambient medium.

In Table 2 we have divided the 87 cycle-24 HCMEs with metric type II radio emission into CMEs with and without a "Delayed" gamma-ray component. The existence of the metric type II radio burst indicates that a shock forms early, making these HCMEs good candidates for SGRE production. We investigated how many of the metric type II-associated HCMEs are with and without a DH type II radio burst or a major SEP event. We selected major SEP events as they are intense events and could have enhancements of >300 MeV protons, which are unlikely to be present in inherently low-intensity SEP events. Because the observer's connection to the SEP source affects the possibility to detect SEPs, the group without a major SEP event could still contain events that were able to accelerate particles, especially the poorly connected eastern hemisphere events could have produced high-energy particles that were not detected. We account for this possibility by using GOES >10 MeV equivalent STEREO intensities to identify major SEP events observed by STEREO. The STEREO >10 MeV flux is estimated using data from the STEREO/HET (von Rosenvinge et al. 2008), which covers the energy ranges of 13–100 MeV. The flux is estimated by fitting a power law to HET data points and integrating the flux in the 10–150 MeV range (see Gopalswamy et al. 2016). In Tables 2 and 3, we have separated the two SEP event sets and marked the one containing both GOES and STEREO events as "(w/STEREO)," although in Table 3 the statistics for the SGRE events are mostly too low. One should note that STEREO spacecraft drift around the Sun, so their magnetic connection to the Sun changes continuously. In addition, STEREO-A observations have significant data gaps during the solar conjunction period during 2014–2015, and contact with STEREO-B was lost on 2014 October 1. We surveyed also STEREO/WAVES data for additional DH type II radio bursts but we found only one on 2011 August 3. The STEREO-A data showed a short-duration, slanted feature in the 10–14 MHz frequency range starting at 13:38 UT, which we added to our DH type II burst list. All other STEREO/WAVES DH type II bursts were accompanied by a Wind/WAVES DH type II burst, so we studied STEREO and Wind DH type II bursts together. The most western event of the seven SGRE events without a major GOES SEP event occurred at the heliographic longitude W18 and four of the seven SGRE events

occurred less than 30° from the eastern limb. The two bottom rows of Table 2 are difficult to interpret, but we have added them mainly for completeness. Results show that all HCMEs associated with an SGRE event have similar average initial acceleration values(1.70–1.85 km s^{-2}) with the exception of the group without a GOES or STEREO SEP event, which contains only three events and the average initial acceleration (2.68 km s^{-2}) is very high, possibly indicating missed major SEP event identification. The range is considerably higher than those of HCMEs without an SGRE event (1.07–1.15 km s^{-2}). The SGRE and SEP-associated HCMEs have the highest average space speed, whereas two groups of HCMEs, SGRE-associated HCMEs without an SEP event and SEP-associated HCMEs without an SGRE event, seem to have similar speeds. However, the average initial accelerations of SGRE-associated HCMEs without a major SEP event are higher (even when we ignore the group without a GOES or STEREO SEP event that has only three events in total) than those without an SGRE event but with a major SEP event. The DH type II-associated HCMEs without an SGRE event have only slightly lower average space speed (1211 km s^{-1}), but we know that DH type II bursts are associated with SEP events and this mixed population includes 12 HCMEs with an SEP event, which have high space speeds. If we exclude these 12 SEP-associated events, then the average space speed of the remaining 25 events decreases to 1064 km s^{-1}. Clearly, the existence of >300 MeV protons is connected to a high initial acceleration and speed of the associated HCME. The HCMEs without an SEP and SGRE event have the lowest average speed (992 km s^{-2}). Therefore, the SGRE-associated HCMEs conform to the hierarchy between the initial acceleration and speed of the CME and the fluence spectral index as described by Gopalswamy et al. (2016). Especially the high initial acceleration seems to be crucial for SGRE production.

The average accelerations and speeds of the 20 cycle-24 HCMEs associated with only a DH type II radio burst are shown in Table 3. HCMEs are mostly without SGRE events (only four SGRE events) or major SEP events (only six SEP events if STEREO observations are included, two of which have also an SGRE event). Therefore, statistics for SGRE events are low, but the average space speed of SGRE events without an SEP event (≈1579 km s^{-1}) is below the space speed of the SGRE events with an SEP event (≈2004 km s^{-1}; ≈1858 km s^{-1} if STEREO observations are included) in Table 2. None of the three eruptions without a major SEP event detected by GOES were magnetically well-connected to Earth, so they probably accelerated high-energy particles efficiently but particles did not reach Earth. One of them, the 2014 June 10 HCME with a solar source at S17E82, actually had a major SEP event observed by STEREO-B, which was located at the heliographic longitude E164. The 2012 March 5 HCME had a solar source at N17E52, but the GOES-equivalent >10 MeV intensities observed by STEREO-B at longitude E117 were already elevated above 100 pfu due to a preceding HCME on March 4 that was not associated with an SGRE event. At the onset of the 2012 March 10 HCME launched from N17W24, the >10 MeV intensities were elevated above 10 pfu at all three spacecraft. In fact, the March 5 and 10 events are the first and last events in a cluster of four SGRE events accompanied by a high level of SEP flux (Gopalswamy et al. 2019). So, it is quite possible that the two 2012 March events also accelerated particles. The average initial acceleration value is lower than the respective value for SGRE events with SEP events in Table 2, but this is expected because CMEs associated with only a DH type II radio burst accelerate slowly and the shock forms later. This probably explains the lower average space speed near the Sun. The initial acceleration and average space speed of HCMEs without an SGRE event and an SEP event are lower or similar, respectively, to the respective values in Table 2. Table B1 in the Appendix lists the data for events included in calculations of Tables 2 and 3.

5. Radial Distance of the Shock at the End of the SGRE Events

We selected two SGRE events, the 2012 January 23 and March 7 events, with the longest duration of the associated type II radio burst (Gopalswamy et al. 2019) and for which the STEREO observations provided side view white-light images of the HCMEs.

The 2012 January 23 04:00 UT HCME produced a DH type II burst with a duration of about 25.0 ± 9.6 hr, while the estimated duration of the SGRE event was 15.4 ± 0.8 hr. The SGRE ended around 19:25 UT. The estimated space speed was 2511 km s^{-1}, and the interplanetary shock arrived at the SOHO spacecraft at 14:33 UT on January 24. The eruption was associated with an M8.7 X-ray flare starting at 03:38 UT at the heliographic location of N28W21. The STEREO-A and STEREO-B longitudes were W108 and E114, respectively. The eruption produced a major SEP event at Earth with a GOES >10 MeV peak proton flux 6310 cm^{-2} s^{-1} sr^{-1}. The 2012 January 23 eruption close to the Sun has been studied extensively because the eruption involved two flux ropes that merged below the radial distance of 15 $R_\odot$ (e.g., Cheng et al. 2013; Joshi et al. 2013; Li & Zhang 2013).

The second HCME at 00:24 UT on 2012 March 7 was associated with an SGRE event that had an even longer duration, about 21.3 ± 1.6 hr (Ajello et al. 2014; Gopalswamy et al. 2018). The 2012 March 7 SGRE had a slightly longer estimated duration of about 21 hr but the SGRE durations cannot be measured accurately because LAT does not observe the Sun continuously. The SGRE end time was 21:40 UT. The estimated duration of the DH type was 27.9 ± 6.8 hr. The LASCO space speed of the HCME was 3146 km s^{-1}, and it was associated with am X5.4 X-ray flare at 00:02 UT from N17E27. A second X1.3-class flare started about an hour later at 01:05 UT. The associated HCME at 01:30 UT had a slightly slower space speed of 2160 km s^{-1}. The STEREO-A and STEREO-B longitudes were W109 and E118, respectively. The SOHO shock arrival time was at 10:53 UT on March 08. The GOES >10 MeV peak proton flux was 6530 cm^{-2} s^{-1} sr^{-1}. The onset of the HCME has been studied by Chintzoglou et al. (2015) and the heliospheric propagation by Patsourakos et al. (2016) and Soni et al. (2023).

5.1. Distance Estimation

We estimated the radial distance and the space speed of the shock by forward fitting a spheroidal shock model to white-light images of STEREO/HIs (Eyles et al. 2009) around the end time of the SGRE event. For shock fitting, we used IDL programs in the Solar Corona Ray-Tracing Software package developed to forward modeling of structures of the solar corona (e.g., Thernisien et al. 2009).[9]

[9] https://soho.nascom.nasa.gov/solarsoft/stereo/secchi/idl/scraytrace/

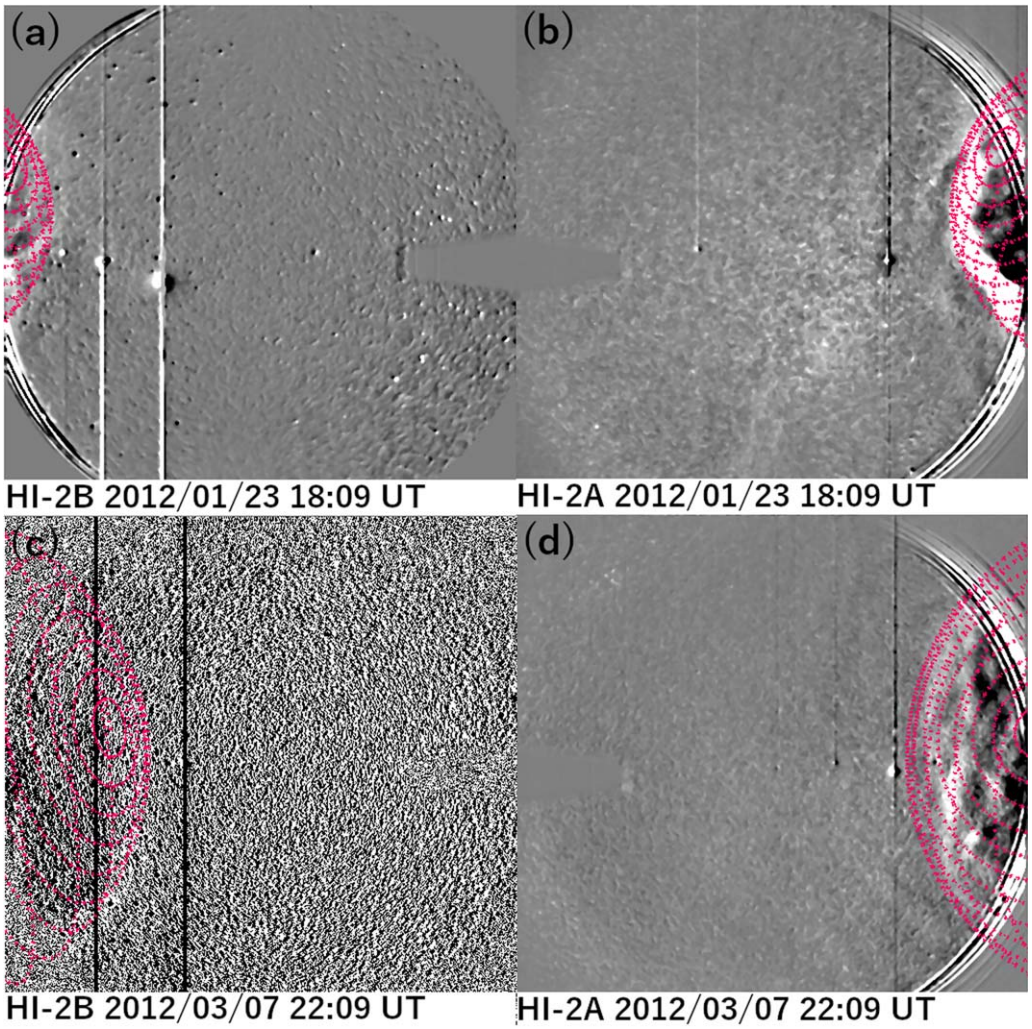

Figure 2. Spheroidal shock fits (red lines) onto the STEREO/HI images of the 2012 January 23 CME (top row) and the 2012 March 7 CME (bottom row).

The fitting of the spheroidal shock model to HI observations is shown in Figure 2. The propagation direction of the shock is difficult to estimate, our estimates were N25W05 for the 2012 January 23 CME and N34E27 for the 2012 March 7 CME. For the 2012 January 23 HCME we obtained the radial distance $r = 121\ R_\odot$, and the space speed 975 km s^{-1}. In the case of the 2012 March 7 HCME the estimated radial $r = 140\ R_\odot$, and the space speed 750 km s^{-1}. The obtained speeds are reasonably high for a strong CME-driven shock to exist.

We compared these results with radial distances estimated using Wind/WAVES observations of the type II radio burst. First, we measured the mid-frequency of the type II emission lane at the time the CME leading edge was around 20 $R_\odot$ because type II emissions are often very complex and overlapped by more intense type III emission during the early phase of the eruption, which makes radio measurements at frequencies corresponding the shock distances close to the Sun difficult. From the frequency formula $f_{\rm plasma} = 9.0 \times \sqrt{N \times n(r)}$, where the radial distance r is in units of $R_\odot$ and frequency f in kHz, we calculated the multiplier N for the Leblanc density model $n(r)$ (Leblanc et al. 1998). The measurement time was obtained by extrapolating the CME height-time profiles obtained by forward fitting a flux rope model to LASCO and SECCHI/COR images to a radial distance of 20 $R_\odot$.

We then estimated the radial distance at the SGRE end time from the mid-frequency of the type II emission lane: For the 2012 January 23 HCME we obtained the multiplier $N = 4.51$, which then gave for the mid-frequency $f = 83$ kHz the radial distance of $r = 132\ R_\odot$. For the 2012 March 7 HCME the respective values were $N = 9.07$, $f = 90$ kHz, and $r = 173\ R_\odot$. The distances estimated from the radio bursts data are 9% and 24% larger than those estimated from the STEREO/HI images. The STEREO/HI height-time measurements are complicated because the actual shape, location, and propagation direction of the shock ahead of the CME body are difficult to discern from the white-light images. The CME structure in white-light is also transparent, so we may confuse structures (e.g., Scott et al. 2019) and brightness depends on local density and Thomson-scattering geometry (Howard & Tappin 2009; Xiong et al. 2013). On the other hand, type II radio emissions are sporadic and depend on local density at the radio source, which the general density model cannot capture. We also assume that the location of the radio source is at the shock nose (e.g., Mäkelä et al. 2018) and the type II emission in interplanetary space occurs at the fundamental of the plasma frequency (Lengyel-Frey et al. 1985).

6. Discussion

In the first part of our analysis, we showed that the near-Sun kinematics of the CMEs correlate with the properties of the gamma-ray emission observed by Fermi/LAT. The population of the CMEs (total of eight CMEs) that were associated with a gamma-ray event whose light curve indicated both "Prompt" and "Delayed" emission components, as defined by Ajello et al. (2021), had the highest average initial acceleration ($1.87\,\mathrm{km\,s^{-2}}$) and fastest average space speed ($1753\,\mathrm{km\,s^{-1}}$). The mixed "Delayed" category, where the existence of the "Prompt" component is uncertain due to the lack of LAT measurements around the flare onset, has a similar average space speed ($1745\,\mathrm{km\,s^{-1}}$) but somewhat lower initial acceleration ($1.73\,\mathrm{km\,s^{-2}}$). The lowest average values ($1.37\,\mathrm{km\,s^{-2}}$ and $775\,\mathrm{km\,s^{-1}}$, respectively) had the population of CMEs (total of six CMEs) associated with gamma-ray flares showing a "Prompt" emission component only, i.e., there were no SGRE emissions detected by LAT. The speeds correspond well with those obtained by Winter et al. (2018) who studied CME properties for X-class flares with and without gamma-ray emission. They found a median CME linear speed of $768\,\mathrm{km\,s^{-1}}$ for X-class flares without gamma-ray emission. If Fermi detected gamma rays during the X-class flare, the median speed of the associated CMEs was $1828\,\mathrm{km\,s^{-1}}$. CMEs associated with SGRE events had the highest median speed of $2125\,\mathrm{km\,s^{-1}}$. The definition of SGRE in their study was that the >100 MeV gamma-ray duration is $\gtrsim$~2 hr. Ajello et al.'s (2021) definition used here is based on details of hard X-ray and gamma-ray light curves, which probably explains why Winter et al.'s (2018) SGRE events were associated with faster CMEs.

In addition, we divided cycle 24 on-disk HCMEs associated with type II radio bursts into groups with and without (a) SGRE events, (b) DH type II bursts, and (c) major SEP events observed. For SEP events we analyzed major events observed by GOES only and the second group of major SEP events observed by GOES or STEREO spacecraft. Our statistical analysis shows that all metric type II-associated HCMEs with an SGRE event have considerably higher initial acceleration and space speed if a major SEP event was also detected than those of metric type II-associated HCMEs without an SGRE event. The average space speeds of the SGRE-associated HCMEs without an SEP event and the non-SGRE-associated HCMEs with a major SEP event were similar. The analysis of the HCMEs associated with only DH type II emission shows that the three SGRE-producing HCMEs without an SEP event observed by GOES spacecraft have higher space speeds than any studied population of HCMEs not associated with an SGRE event. However, one of those three HCMEs had a major SEP event observed by STEREO-B and the other two had elevated backgrounds at least at the best connected spacecraft, so all three events that could have accelerated protons. Whereas the average initial acceleration is slightly lower than those of the metric type II-associated HCMEs without an SGRE event, but clearly higher than those of the DH type II-associated HCMEs without an SGRE event. The lower value is expected because CMEs associated with only a DH type II radio burst accelerate slowly and the shock forms later. This result resembles the kinematic hierarchy of CMEs with major SEP events, where rare, slowly accelerating but eventually fast CMEs associated with filament eruptions outside active regions can produce large SEP events at 1 au. In the case of filament eruptions, we know that the resulting energy spectrum is soft, but the general idea is that occasionally the initial acceleration of the CME is slower, but acceleration continues long enough so that a sufficiently strong shock forms later at higher altitudes is comparable. In general, our results are similar to those reported by Gopalswamy et al. (2022a). The SGRE-associated HCMEs seem to conform to the hierarchy between the initial acceleration and speed of the CME and the fluence spectral index as described by Gopalswamy et al. (2016). Clearly, the existence of >300 MeV protons is connected to high initial acceleration and speed of the associated HCME. Therefore, our results suggest that CME-driven shocks are the likely source for the >300 MeV protons required to produce SGREs at the Sun.

The mirror effect near the Sun limits the number of protons that can penetrate deep enough, i.e., particles with a pitch angle α in the sheath region cannot penetrate a near-Sun region if $\mu = \cos\alpha$ is larger than the critical value μ_c:

$$|\mu| \geqslant \mu_c \equiv \sqrt{1 - \frac{B_{\mathrm{sheath}}}{B_\odot}}. \quad (1)$$

Because the foot points of the field lines crossing the shock nose could be connected to areas outside the source active region where the average magnetic field strength $B_\odot$ is considerably lower than in active regions, the mirror ratio $B_{\mathrm{sheath}}/B_\odot$ increases and the width of the loss cone $\alpha_c = \cos^{-1}\mu_c = \sin^{-1}\sqrt{B_{\mathrm{sheath}}/B_\odot}$ becomes larger. Because the CME flux ropes have a pile-up region in front of them, the magnetic field within the sheath could be significantly larger than the ambient field, which will further lower the mirror ratio. Therefore, more protons can precipitate deep into the solar atmosphere. As mentioned earlier, enhanced turbulence increases scattering into the loss cone, which in turn increases the number of precipitating particles at the foot points. The level of the turbulence and its time evolution along the flux-rope-wrapping field lines and in the atmospheric layers close to the Sun are difficult to estimate. For example, EUV waves associated with large solar eruptions and propagating long distances over the solar surface clearly indicate that coronal shocks and CME lateral expansion affect the solar atmosphere far from the eruption site, most likely resulting in large volumes of enhanced turbulence around the source active region.

It should be noted that fast CME shocks are the only sites for which we have clear corroborating observational evidence for an acceleration of >300 MeV protons over extended times long after the end of the solar flare. Winter et al. (2018) studied the properties of the soft X-ray flares, CMEs, and SEP events associated with SGRE events. They found that SGRE events are not produced by the brightest, most intense X-ray flares. In their reverse study, they found that during the period from 2011 March to 2015 June 45 X-class soft X-ray flares were detected, but only 15 of those were associated with an SGRE event. Similarly, their study showed that SGRE events are associated with fast CMEs and the SGRE duration increases as the CME speed increases. The reverse study of the fast HCMEs with speeds above $1500\,\mathrm{km\,s^{-1}}$ found only four HCMEs without a reported gamma-ray event. Two of the four HCMEs, the 2011 September 22 10:48 UT and 2012 July 19 05:24 UT halos, had concurrent Fermi/LAT observations. In both events, the LAT spectra showed slight increases that were not significant enough to be characterized as detection. In the study of related SEP events observed by GOES, Winter et al. (2018) list only the 2011 March 7 SGRE event as magnetically well-connected to GOES and without a significant background increase due to a

preceding event but did not show any increase in the GOES >300 MeV flux. Gopalswamy et al. (2019) suggest that the lack of high-energy protons is due to a poor latitudinal magnetic connection of the shock nose to Earth because the flare occurred at the heliographic latitude of N31 and the northern polar region of the Sun is tilted away from Earth in March. Similarly, Gopalswamy et al. (2022b) showed that the soft energy spectrum observed by GOES during the 2014 January 7 SGRE event was due to poor magnetic connectivity of the shock nose to an Earth observer. The final conclusion of Winter et al. (2018) is that their results favor the CME shock as the source of the SGRE-producing protons.

The >300 MeV protons are accelerated near the nose of the CME-driven shock (e.g., Gopalswamy et al. 2013; Gopalswamy & Mäkelä 2014; Gopalswamy et al. 2014), with a possible exception of the earliest phase of the eruption, where the fast lateral expansion of the shock could result in efficient particle acceleration away from the nose region. Some fraction of the shock-accelerated protons escape into the IP space and are detected as an SEP event, but others propagate along the magnetic field lines deep down into the solar atmosphere and generate SGRE. In addition, the magnetic field lines that are pushed ahead of the CME body maintain a continuous connection between the shock and the solar atmosphere. Therefore, if the shock can accelerate protons to energies >300 MeV, protons will have a propagation path back to the Sun and can generate SGREs. The key aspect of the CME-shock model is that the magnetic field lines protons travel along sunward cross the shock front into the sheath region behind the shock, wrap around the CME flux rope and connect back to the Sun in areas outside the foot points of the CME flux rope and possibly also areas outside the source active region. Therefore, the locations of the foot points are widely separated providing a natural explanation for the spatially extended source of gamma-ray emission.

We estimated the radial distance of the CME-driven shock at the end time of the SGRE event for the 2012 January 23 and 2012 March 7 SGRE events. These events were associated with the two longest-duration type II radio bursts. We estimated the shock radial distance by forward fitting a spheroidal shock model to STEREO/HI white-light images of the CME and obtained for the 2012 January 23 SGRE event the shock radial distance $r = 121\ R_\odot$ and for the 2012 March 7 SGRE event $r = 140\ R_\odot$. In addition, we used the frequency of the type II radio burst obtained from the radio dynamic spectra of Wind/WAVES together with a radial density model to get another estimate for the shock radial distance. The obtained distances from radio measurement were slightly longer, for the 2012 January 23 SGRE event $r = 132\ R_\odot$, and for the 2012 March 7 SGRE event $r = 173\ R_\odot$.

Patsourakos et al. (2016) estimated the speed of the 2012 March 7 CME using the standard aerodynamic drag-force model approach, where the CME traveled through the quiet or perturbed solar wind (SW). Based on their results (their Figure 8), the estimated speed of the CME at 22 UT for the quiet SW model was $\approx$740 km s^{-1} and for the perturbed SW model $\approx$820 km s^{-1}. The perturbed SW model matches better the CME arrival time and speed at the Wind spacecraft. Therefore, our estimated CME speed of 750 km s^{-1} seems to be slightly below the one obtained from the perturbed SW model. Recently, Soni et al. (2023) studied the arrival signatures of the 2012 March 7 CME at several heliospheric locations. They report that Venus Express detected the arrival of the CME ejecta at 13:28 UT when Venus was at the radial distance of 154 $R_\odot$. Therefore, the radial distance estimated from the forward fitting of the spheroidal shock model, $r = 140\ R_\odot$, is clearly too low, and most likely the radial distance obtained from radio observations, $r = 173\ R_\odot$, is closer to the actual distance. The model fitting to images of the 2012 March 7 CME was difficult because the CME structure was very faint in the STEREO-B images (see Figure 2(c). Therefore, the sensitivity of the imaging system may not be high enough to detect the shock in front of the CME.

The estimation of the radial distance of the shock at the end time of the SGRE event is quite complicated. The location and the shape of the shock front are difficult to discern from white-light images of the CME (e.g., Odstrcil & Pizzo 2009; Scott et al. 2019). CMEs are transparent structures, and the intensity of Thomson scattering depends on viewing angle relative to the structure. The location of the type II radio source on the shock front is also difficult to measure. Imaging radio instruments operate at higher frequencies, which correspond to heights of a couple solar radii above the solar surface. Direction finding and triangulation can be used to locate the interplanetary type II radio sources at lower frequencies. However, the scattering of radio waves and low intensity of type II emission limit the accuracy of the direction-finding measurements.

The CME-driven shock in both events reached SOHO spacecraft (2012 January 24 14:33 UT and 2012 March 08 10:53 UT respectively) and when shocks passed 1 au about 30 minutes later, GOES spacecraft observed a clear increase around the shock time visible in Figure 3. Both events had a particle flux increase in the GOES 350–429 MeV channels indicating that the CME-driven shock did accelerate >300 MeV protons. In both cases the 1 au enhancement continued beyond the end times of the SGRE events, estimated to be at the 2012 January 23 19:25 UT and 2012 March 7 21:40 UT, respectively. During the March 7 event, the particle increase was detectable at even higher energies, up to the 510–700 MeV energy range. The event integrated fluence spectrum of 2012 January 23 event provided by PAMELA indicates that the SEP flux at 1 au extended above 300 MeV (Bruno et al. 2018). Therefore, the CME-driven shock clearly must accelerate >300 MeV protons far away from the Sun, providing support for the CME shock as the source of the SGRE-producing protons.

The 2012 March 7 SGRE event was so bright that the location of the >100 MeV gamma-ray emission source could be estimated over several time intervals over a period of about 10 hr (Ajello et al. 2014, 2021). The emission centroid seemed to move away from the flare site across the solar toward the west. Ajello et al. (2021) studied two other, bright SGRE flares on 2014 February 25 and 2017 September 10. The gamma-ray intensity of the 2014 February flare was weaker, so they could determine the location of the emission centroid only during two intervals over 3 hr. The September 2017 flare was brighter, and the location was determined in three intervals over 7 hr, but the flare occurred over the western limb of the Sun making the detection of possible source movement difficult. In both events, the centroid remained consistent with the AR location. Therefore, the movement of the SGRE source during the 2012 March 7 event supports CME-shock scenario, whereas the detection of a possible source movement in the 2014 February 25 and 2017 September 10 events is complicated because of the weaker gamma-ray intensity or unfavorable location of the flare.

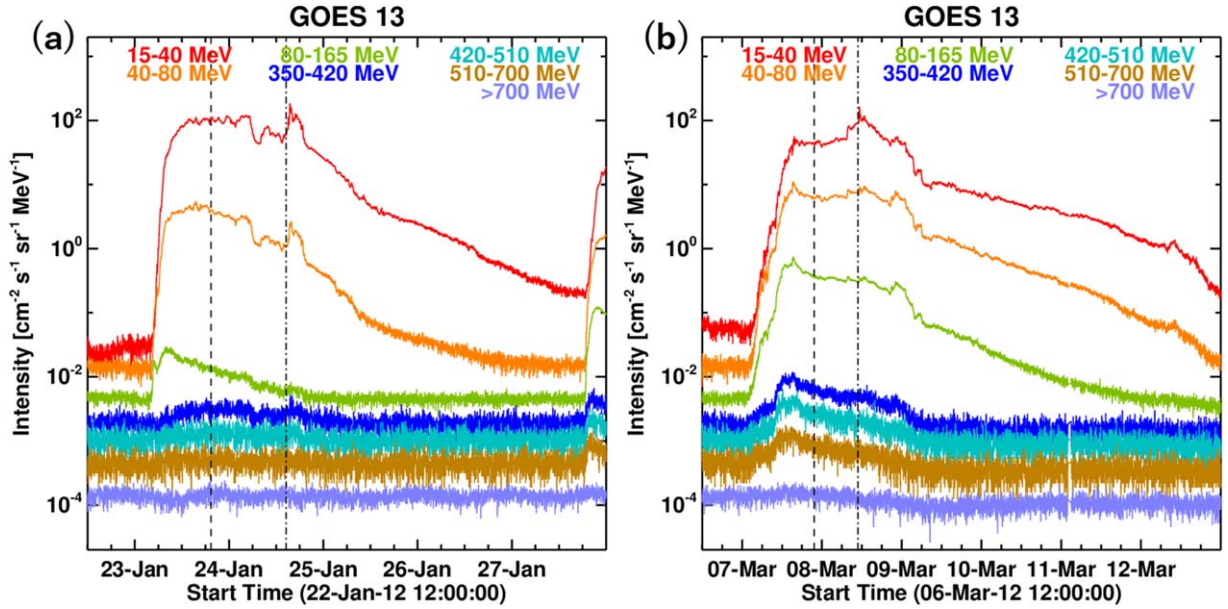

Figure 3. GOES-13 measurements of the SEP events associated with the 2012 January 23 (a) and 2012 March 7 CMEs and SGRE events. Both events show enhanced intensity in the 350–420 MeV channel (blue). The March 7 event has a clear flux increase in the higher-energy 510–700 MeV channel (brown). The estimated SGRE end times at 2012 January 23 19:25 UT and March 7 21:40 UT are marked by dashed lines and the SOHO shock times at 2012 January 24 14:33 UT and March 08 10:53 UT by dashed–dotted lines.

7. Conclusions

We compared acceleration and speed of CMEs associated with gamma-ray flares with the "Prompt" and/or "Delayed" (SGRE event) components as defined by Ajello et al. (2021). In addition, we divided the on-disk HCMEs associated with type II radio bursts into groups with or without SGRE events, SEP events, metric, or DH type II radio bursts and compared the average acceleration and speed between the HCME groups. We showed that the CMEs associated with the "Delayed" gamma-ray component and the metric type II-producing HCMEs associated with SGRE events together with a DH type II radio burst and/or major SEP events have higher initial acceleration and space speed than the CMEs associated with the "Prompt Only" gamma-ray component or the SEP- or type II-associated HCMEs without SGRE. The only exception was the space speed of metric type II -associated HCMEs with a major SEP event but without an SGRE event that had similar average space speeds as the SGRE-associated HCMEs without a major SEP event. Similar high initial acceleration and fast speed characteristics are shared by CMEs associated with GLEs, which are guaranteed to have >300 MeV protons. The SGRE-associated CMEs also conform to the hierarchy between the initial acceleration and speed of the CME and the fluence spectral index as described by Gopalswamy et al. (2016). Therefore, our findings support the CME-driven shock as the source of >300 MeV protons producing SGRE events.

We estimated the radial distance the CME-driven shock at the end time of the SGRE event with the long-duration type II radio bursts on 2012 January 23 and 2012 March 7 using STEREO/HI white-light images of the CME and radio dynamic spectra of Wind/WAVES. The shock radial distances for the 2012 January 23 SGRE event were $r = 121\ R_\odot$ and $r = 132\ R_\odot$, and for the 2012 March 7 SGRE event $r = 140\ R_\odot$ and $r = 173\ R_\odot$, respectively. The distances derived from white-light and radio observations are reasonably consistent, indicating that the radio source is near the shock nose as assumed. The distances are also consistently longer than the estimated shock height ≈70 $R_\odot$ for the shorter-duration 2014 February 25 SGRE event Gopalswamy et al. (2019). Because the shock location is not visible in the white-light images, the radial distance estimated from forward fitting of the spheroidal shock model is probably underestimated. At the end time of the SGRE event, the shock speeds were still high enough (975 km s^{-1} and 750 km s^{-1}) for high-energy particle acceleration. Therefore, we conclude that strong CME-driven shocks accelerate >300 MeV protons up to the radial distances of 0.6–0.8 au.

Acknowledgments

We thank the Fermi/LAT, GOES, SOHO/LASCO, STEREO/SECCHI, Wind/WAVES, and HELCATS teams for providing the data. P.M. and S.A. were partially supported by NSF grant AGS-2043131. N.G. was supported by NASA's STEREO project and the Living With a Star program. H.X. was partially supported by NSF grant AGS-2228967.

Appendix A
CMEs and X-Ray Flares Associated with On-disk Fermi/LAT Solar Flares

Table A1 contains data for the CME and X-ray flare data used in Table 2. The first column gives the first observation date and time of the CME followed by the measured sky-plane speed and the projection-corrected space speed in the second and third columns. The fourth column lists the estimated initial acceleration of the CME. Columns 5–7 list the location in heliographic coordinates, the onset, and the peak times of the GOES soft X-ray flare. The last column lists the gamma-ray components detected by Fermi/LAT taken from Ajello et al. (2021).

Table A1
CME and X-Ray Flare Data for Fermi/LAT Solar Flares

CME (UT) (1)	Sky Speed (km $^{-1}$) (2)	Space Speed (km s^{-1}) (3)	Acc (km s^{-2}) (4)	Location (UT) (5)	Flare Onset (UT) (6)	Flare Peak (UT) (7)	Gamma-ray Components (8)
2010/06/12 01:31	620	674	0.42	N23W43	2010/06/12 00:30	2010/06/12 00:57	LLE-Prompt
2011/03/07 20:00	2125	2223	1.28	N30W48	2011/03/07 19:43	2011/03/07 20:12	Delayed
2011/06/07 06:49	1255	1321	0.88	S21W54	2011/06/07 06:16	2011/06/07 06:41	Delayed
2011/08/04 04:12	1315	1477	1.54	N19W36	2011/08/04 03:41	2011/08/04 03:57	Delayed
2011/08/09 08:12	1610	1640	1.61	N17W69	2011/08/09 07:48	2011/08/09 08:05	Prompt Short-Delayed
2011/09/06 23:05	575	830	1.73	N14W18	2011/09/06 22:12	2011/09/06 22:20	LLE-Prompt Short-Delayed
2011/09/07 23:05	710	735	2.04	N14W28	2011/09/07 22:32	2011/09/07 22:38	Delayed
2011/09/24 09:48	1936	2235	1.96	N12E60	2011/09/24 09:21	2011/09/24 09:40	LLE-Prompt Short-Delayed
2012/01/23 04:00	2175	2511	1.99	N28W21	2012/01/23 03:38	2012/01/23 03:59	Delayed
2012/01/27 18:27	2508	2541	0.71	N27W78	2012/01/27 17:37	2012/01/27 18:37	Delayed
2012/03/05 04:00	1531	1627	0.52	N17E52	2012/03/05 03:17	2012/03/05 04:09	Delayed
2012/03/07 00:24	2684	3146	2.38	N17E27	2012/03/07 00:02	2012/03/07 00:24	Delayed
2012/03/09 04:26	950	1229	0.66	N15W03	2012/03/09 03:22	2012/03/09 03:53	No-Prompt Delayed
2012/03/10 18:00	1296	1638	0.94	N17W24	2012/03/10 17:15	2012/03/10 17:44	Delayed
2012/05/17 01:48	1582	1596	1.21	N11W76	2012/05/17 01:25	2012/05/17 01:47	Delayed
2012/06/03 18:12	772	786	1.87	N16E38	2012/06/03 17:48	2012/06/03 17:55	LLE-Prompt Short-Delayed
2012/07/06 23:24	1828	1907	4.54	S13W59	2012/07/06 23:01	2012/07/06 23:08	Delayed
2012/08/06 05:12	198	199	0.66	S14E84	2012/08/06 04:33	2012/08/06 04:38	LLE-Prompt
2012/11/13 02:24	980	1002	2.78	S25E46	2012/11/13 01:58	2012/11/13 02:04	Prompt
2013/04/11 07:24	861	1369	1.09	N09E12	2013/04/11 06:55	2013/04/11 07:16	No-Prompt Short-Delayed
2013/05/13 02:00	1270	1270	0.88	N11E90	2013/05/13 01:53	2013/05/13 02:17	Delayed
2013/05/13 16:07	1850	1852	1.82	N11E85	2013/05/13 15:48	2013/05/13 16:05	Delayed
2013/05/14 01:25	2625	2645	4.01	N08E77	2013/05/14 01:00	2013/05/14 01:11	No-Prompt Delayed
2013/05/15 01:48	1366	1408	0.71	N12E64	2013/05/15 01:15	2013/05/15 01:48	No-Prompt Delayed
2013/10/25 08:12	587	599	1.25	S08E73	2013/10/25 07:53	2013/10/25 08:01	Delayed
2013/10/28 02:24	695	726	0.55	N04W66	2013/10/28 01:41	2013/10/28 02:03	LLE-Prompt
2013/10/28 04:48	1201	1270	2.35	N08W71	2013/10/28 04:32	2013/10/28 04:41	LLE-Prompt
2013/10/28 15:36	812	1098	2.29	S06E28	2013/10/28 15:07	2013/10/28 15:15	Delayed
2013/10/28 21:25	771	777	1.44	N07W83	2013/10/28 20:48	2013/10/28 20:57	LLE-Prompt
2014/01/07 18:24	1830	2246	1.34	S15W11	2014/01/07 18:04	2014/01/07 18:32	Delayed
2014/02/25 01:25	2147	2153	3.59	S12E82	2014/02/25 00:39	2014/02/25 00:49	LLE-Prompt Delayed
2014/06/10 13:30	1469	1473	1.53	S17E82	2014/06/10 12:36	2014/06/10 12:52	LLE-Prompt Delayed
2014/06/11 09:24	829	915	2.18	S18E65	2014/06/11 08:59	2014/06/11 09:06	Short-Delayed
2014/09/10 18:00	1267	1652	1.15	N14E02	2014/09/10 17:21	2014/09/10 17:45	Short-Delayed
2015/06/21 02:36	1366	1740	0.97	N12E16	2015/06/21 02:06	2015/06/21 02:36	Prompt Delayed
2015/06/25 08:36	1627	1805	2.15	N09W42	2015/06/25 08:02	2015/06/25 08:16	Delayed
2017/09/06 12:24	1571	1819	3.37	S08W33	2017/09/06 11:53	2017/09/06 12:02	Delayed
2017/09/10 16:00	3163	3163	1.70	S09W92	2017/09/10 15:35	2017/09/10 16:06	Prompt Delayed

Note. Gamma-ray Components are taken from Ajello et al. (2021).

Appendix B
Cycle 24 HCMEs with Type II Radio Bursts and On-disk X-Ray Flares

Table B1 contains data for the cycle-24 HCME and X-ray flares used in Tables 2 and 3. Columns 1–7 are the same as in Table A1. Columns 8–9 list the onset times of the reported metric and DH type II radio bursts. The DH type II onset times are listed for Wind/WAVES, except on 2011 August 3, when only STEREO-A/WAVES detected a DH type II burst. Column 10 indicates on which spacecraft the WAVES instruments could detect a DH type II radio burst (W = Wind, A = STEREO-A, B = STEREO-B, "–" = no report). Columns 11–12 mark if the event had a major SEP event (G = GOES, A = STEREO-A, B = STEREO-B, "–" = data gap) and an SGRE event ("Delayed" component detected), respectively.

Table B1
Cycle 24 HCMEs with Type II Radio Bursts

HCME (UT) (1)	Sky Speed (km s^{-1}) (2)	Space Speed (km s^{-1}) (3)	Acc (km s^{-2}) (4)	Location (5)	Flare Onset (UT) (6)	Flare Peak (UT) (7)	m-Type II (UT) (8)	DH Type II (UT) (9)	WAVES S/C (10)	SEP G/A/B (11)	SGRE (12)
2010/08/01 13:42	850	1030	0.34	N20E36	2010/08/01 07:36	2010/08/01 08:26	⋯	2010/08/01 09:20	W/A/B	0/-/0	0
2010/08/07 18:36	871	1102	0.63	N11E34	2010/08/07 17:55	2010/08/07 18:24	2010/08/07 18:08	2010/08/07 18:35	W/A/B	0/0/1	0
2010/08/14 10:12	1205	1280	0.51	N17W52	2010/08/14 09:23	2010/08/14 10:05	2010/08/14 09:52	⋯	-/-/-	1/0/0	0
2011/02/14 18:24	326	544	1.51	S20W04	2011/02/14 17:20	2011/02/14 17:26	2011/02/14 17:28	⋯	-/-/-	0/0/0	0
2011/02/15 02:24	669	960	1.33	S20W10	2011/02/15 01:44	2011/02/15 01:56	2011/02/15 01:52	2011/02/15 02:10	W/A/B	0/0/1	0
2011/03/07 20:00	2125	2223	1.28	N30W48	2011/03/07 19:43	2011/03/07 20:12	2011/03/07 19:54	2011/03/07 20:00	W/A/-	1/1/0	1
2011/06/02 08:12	976	1147	0.64	S19E25	2011/06/02 07:16	2011/06/02 07:46	⋯	2011/06/02 08:00	W/A/B	0/0/0	0
2011/06/07 06:49	1255	1321	0.88	S21W54	2011/06/07 06:16	2011/06/07 06:41	2011/06/07 06:25	2011/06/07 06:45	W/A/B	1/0/0	1
2011/06/21 03:16	719	882	0.12	N16W08	2011/06/21 01:22	2011/06/21 03:25	⋯	2011/06/21 03:07	W/-/-	0/0/0	0
2011/08/03 14:00	610	785	0.37	N16W30	2011/08/03 13:13	2011/08/03 13:48	2011/08/03 13:35	2011/08/03 13:38	-/A/-	0/0/0	0
2011/08/04 04:12	1315	1477	1.54	N19W36	2011/08/04 03:41	2011/08/04 03:57	2011/08/04 03:54	2011/08/04 04:15	W/A/B	1/0/0	1
2011/08/09 08:12	1610	1640	1.61	N17W69	2011/08/09 07:48	2011/08/09 08:05	2011/08/09 08:01	2011/08/09 08:20	W/-/-	1/0/0	1
2011/09/06 02:24	782	1232	1.37	N14W07	2011/09/06 01:35	2011/09/06 01:50	2011/09/06 01:46	2011/09/06 02:00	W/-/-	0/0/0	0
2011/09/06 23:05	575	830	1.73	N14W18	2011/09/06 22:12	2011/09/06 22:20	2011/09/06 22:19	2011/09/06 22:30	W/A/-	0/0/0	1
2011/09/22 10:48	1905	1905	0.99	N09E89	2011/09/22 10:29	2011/09/22 11:01	2011/09/22 10:39	2011/09/22 11:05	W/-/B	1/1/1	0
2011/09/24 12:48	1915	2018	0.58	N10E56	2011/09/24 12:22	2011/09/24 13:20	⋯	2011/09/24 12:50	W/-/B	0/0/0	0
2011/09/24 19:36	972	1076	1.49	N12E42	2011/09/24 19:09	2011/09/24 19:21	2011/09/24 19:14	⋯	-/-/-	0/0/1	0
2011/11/09 13:36	907	1012	0.54	N24E35	2011/11/09 13:04	2011/11/09 13:35	2011/11/09 13:11	2011/11/09 13:30	W/-/B	0/0/0	0
2011/11/26 07:12	933	1001	0.60	N17W49	2011/11/26 06:42	2011/11/26 07:10	⋯	2011/11/26 07:15	W/A/-	1/1/0	0
2012/01/19 14:36	1120	1269	0.15	N32E22	2012/01/19 13:44	2012/01/19 16:05	⋯	2012/01/19 15:00	W/A/B	0/0/1	0
2012/01/23 04:00	2175	2511	1.99	N28W21	2012/01/23 03:38	2012/01/23 03:59	2012/01/23 03:43	2012/01/23 04:00	W/A/-	1/1/1	1
2012/01/27 18:27	2508	2541	0.71	N27W78	2012/01/27 17:37	2012/01/27 18:37	2012/01/27 18:10	2012/01/27 18:30	W/A/B	1/1/0	1
2012/03/05 04:00	1531	1627	0.52	N17E52	2012/03/05 03:17	2012/03/05 04:09	⋯	2012/03/05 04:00	W/A/B	0/0/0	1
2012/03/07 00:24	2684	3146	2.38	N17E27	2012/03/07 00:02	2012/03/07 00:24	2012/03/07 00:17	2012/03/07 01:00	W/A/B	1/0/1	1
2012/03/07 01:30	1825	2160	4.00	N15E26	2012/03/07 01:05	2012/03/07 01:14	2012/03/07 01:09	⋯	-/-/-	0/0/0	0
2012/03/09 04:26	950	1229	0.66	N15W03	2012/03/09 03:22	2012/03/09 03:53	2012/03/09 03:43	2012/03/09 04:10	W/-/-	0/1/0	1
2012/03/10 18:00	1296	1638	0.94	N17W24	2012/03/10 17:15	2012/03/10 17:44	⋯	2012/03/10 17:55	W/A/-	0/0/0	1
2012/03/13 17:36	1884	1931	0.89	N17W66	2012/03/13 17:05	2012/03/13 17:41	2012/03/13 17:15	2012/03/13 17:35	W/A/-	1/0/0	0
2012/04/05 21:25	828	1065	0.66	N18W29	2012/04/05 20:43	2012/04/05 21:10	2012/04/05 21:08	⋯	-/-/-	0/0/0	0
2012/04/09 12:36	921	945	0.38	N20W65	2012/04/09 12:02	2012/04/09 12:44	2012/04/09 12:28	2012/04/09 12:20	W/A/-	0/0/0	0
2012/04/23 18:24	528	769	0.99	N14W17	2012/04/23 17:38	2012/04/23 17:51	2012/04/23 17:42	⋯	-/-/-	0/0/0	0
2012/05/17 01:48	1582	1596	1.21	N11W76	2012/05/17 01:25	2012/05/17 01:47	2012/05/17 01:31	2012/05/17 01:40	W/A/-	1/0/0	1
2012/07/04 17:24	662	830	2.31	N14W34	2012/07/04 16:33	2012/07/04 16:39	2012/07/04 16:42	2012/07/04 17:00	W/-/-	0/0/0	0
2012/07/06 23:24	1828	1907	4.54	S13W59	2012/07/06 23:01	2012/07/06 23:08	2012/07/06 23:09	2012/07/06 23:10	W/A/-	1/0/0	1
2012/07/12 16:48	885	1405	0.51	S15W01	2012/07/12 16:03	2012/07/12 16:49	2012/07/12 16:25	2012/07/12 16:45	W/-/-	1/0/1	0
2012/07/19 05:24	1631	1631	0.37	S13W88	2012/07/19 04:45	2012/07/19 05:58	2012/07/19 05:24	2012/07/19 05:30	W/-/-	1/0/0	0
2012/07/28 21:12	420	463	0.64	S25E54	2012/07/28 20:44	2012/07/28 20:56	2012/07/28 20:52	⋯	-/-/-	0/0/0	0
2012/07/31 11:24	567	605	0.23	N19E59	2012/07/31 10:46	2012/07/31 11:30	2012/07/31 11:04	⋯	-/-/-	0/0/0	0
2012/08/13 13:25	435	705	1.68	N22W03	2012/08/13 12:33	2012/08/13 12:40	2012/08/13 12:41	⋯	-/-/-	0/0/0	0
2012/08/31 20:00	1442	1495	0.35	S19E50	2012/08/31 19:32	2012/08/31 20:43	2012/08/31 19:42	2012/08/31 20:00	W/A/-	1/0/1	0
2012/09/28 00:12	947	1093	0.87	N09W31	2012/09/27 23:36	2012/09/27 23:57	2012/09/27 23:44	2012/09/27 23:55	W/A/-	1/0/1	0
2012/11/08 02:36	855	855	0.95	N13E89	2012/11/08 02:08	2012/11/08 02:23	2012/11/08 02:21	⋯	-/-/-	0/0/0	0
2012/11/21 16:00	529	942	0.79	N05E05	2012/11/21 15:10	2012/11/21 15:30	2012/11/21 15:33	⋯	-/-/-	0/0/0	0
2013/03/15 07:12	1063	1366	0.39	N11E12	2013/03/15 06:00	2013/03/15 06:58	⋯	2013/03/15 07:00	W/-/-	1/0/0	0

Table B1
(Continued)

HCME (UT) (1)	Sky Speed (km s^{-1}) (2)	Space Speed (km s^{-1}) (3)	Acc (km s^{-2}) (4)	Location (5)	Flare Onset (UT) (6)	Flare Peak (UT) (7)	m-Type II (UT) (8)	DH Type II (UT) (9)	WAVES S/C (10)	SEP G/A/B (11)	SGRE (12)
2013/04/11 07:24	861	1369	1.09	N09E12	2013/04/11 06:55	2013/04/11 07:16	2013/04/11 07:02	2013/04/11 07:10	W/-/B	1/0/1	1
2013/05/13 02:00	1270	1270	0.88	N11E90	2013/05/13 01:53	2013/05/13 02:17	2013/05/13 02:10	2013/05/13 02:20	W/-/B	0/0/1	1
2013/05/13 16:07	1850	1852	1.82	N11E85	2013/05/13 15:48	2013/05/13 16:05	2013/05/13 15:57	2013/05/13 16:15	W/A/B	0/0/1	1
2013/05/14 01:25	2625	2645	4.01	N08E77	2013/05/14 01:00	2013/05/14 01:11	2013/05/14 01:07	2013/05/14 01:16	W/A/B	0/0/0	1
2013/05/15 01:48	1366	1408	0.71	N12E64	2013/05/15 01:15	2013/05/15 01:48	2013/05/15 01:37	2013/05/15 01:49	W/-/-	1/0/0	1
2013/05/17 09:12	1345	1412	1.68	N12E57	2013/05/17 08:43	2013/05/17 08:57	2013/05/17 08:50	…	-/-/-	0/0/0	0
2013/05/22 13:25	1466	1491	0.71	N15W70	2013/05/22 12:57	2013/05/22 13:32	2013/05/22 12:59	2013/05/22 13:10	W/A/B	1/1/0	0
2013/06/28 02:00	1037	1254	0.91	S18W19	2013/06/28 01:36	2013/06/28 01:59	…	2013/06/28 01:53	W/-/-	0/0/0	0
2013/08/17 19:12	1202	1418	0.54	S05W30	2013/08/17 18:49	2013/08/17 19:33	2013/08/17 18:56	2013/08/17 20:25	W/-/-	0/0/0	0
2013/08/30 02:48	949	1031	0.31	N15E46	2013/08/30 01:51	2013/08/30 02:46	2013/08/30 02:12	2013/08/30 02:34	W/-/-	0/0/0	0
2013/09/29 22:12	1179	1370	0.21	N17W29	2013/09/29 21:43	2013/09/29 23:31	2013/09/29 21:53	2013/09/29 21:53	W/A/B	1/0/0	0
2013/10/22 21:48	459	1070	3.57	N04W01	2013/10/22 21:15	2013/10/22 21:20	2013/10/22 21:21	2013/10/22 21:33	W/-/-	0/0/0	0
2013/10/24 01:25	399	766	1.42	S10E08	2013/10/24 00:21	2013/10/24 00:30	2013/10/24 00:31	…	-/-/-	0/0/0	0
2013/10/25 08:12	587	599	1.25	S08E73	2013/10/25 07:53	2013/10/25 08:01	2013/10/25 07:59	…	-/-/-	0/0/1	1
2013/10/25 15:12	1081	1103	1.53	S06E69	2013/10/25 14:51	2013/10/25 15:03	2013/10/25 14:58	2013/10/25 15:08	W/-/B	0/0/0	0
2013/10/28 02:24	695	726	0.55	N04W66	2013/10/28 01:41	2013/10/28 02:03	2013/10/28 02:00	…	-/-/-	0/0/0	0
2013/10/28 15:36	812	1098	2.29	S06E28	2013/10/28 15:07	2013/10/28 15:15	2013/10/28 15:10	2013/10/28 15:24	W/-/-	0/0/0	1
2013/10/29 22:00	1001	1001	1.39	N05W89	2013/10/29 21:42	2013/10/29 21:54	2013/10/29 21:48	…	-/-/-	0/0/0	0
2013/11/19 10:36	740	761	1.06	S14W70	2013/11/19 10:14	2013/11/19 10:26	2013/11/19 10:24	2013/11/19 10:39	W/-/-	0/0/0	0
2013/12/07 07:36	1085	1165	1.62	S16W49	2013/12/07 07:17	2013/12/07 07:29	2013/12/07 07:27	2013/12/07 07:43	W/-/-	0/0/0	0
2014/01/07 18:24	1830	2246	1.34	S15W11	2014/01/07 18:04	2014/01/07 18:32	2014/01/07 18:17	2014/01/07 18:33	W/A/B	1/1/1	1
2014/01/20 22:00	721	750	0.18	S07E67	2014/01/20 21:39	2014/01/20 22:49	…	2014/01/20 22:24	W/-/-	0/0/0	0
2014/02/20 08:00	948	960	0.53	S15W73	2014/02/20 07:26	2014/02/20 07:56	2014/02/20 07:45	2014/02/20 08:05	W/-/-	1/0/0	0
2014/02/25 01:25	2147	2153	3.59	S12E82	2014/02/25 00:39	2014/02/25 00:49	2014/02/25 00:56	2014/02/25 00:56	W/A/B	1/1/1	1
2014/03/20 04:36	740	921	1.10	S14E35	2014/03/20 03:42	2014/03/20 03:56	2014/03/20 03:52	…	-/-/-	0/0/0	0
2014/03/29 18:12	528	679	0.87	N11W32	2014/03/29 17:35	2014/03/29 17:48	2014/03/29 17:53	2014/03/29 17:59	W/-/-	0/0/0	0
2014/04/02 13:36	1471	1564	0.55	N11E53	2014/04/02 13:18	2014/04/02 14:05	2014/04/02 13:23	2014/04/02 13:42	W/-/B	0/0/1	0
2014/04/18 13:25	1203	1359	0.71	S20W34	2014/04/18 12:31	2014/04/18 13:03	2014/04/18 12:55	2014/04/18 13:05	W/-/-	1/0/0	0
2014/06/10 13:30	1469	1473	1.53	S17E82	2014/06/10 12:36	2014/06/10 12:52	…	2014/06/10 12:58	W/-/B	0/0/1	1
2014/07/08 16:36	773	841	1.00	N12E56	2014/07/08 16:06	2014/07/08 16:20	2014/07/08 16:14	…	-/-/-	0/-/0	0
2014/08/01 18:36	789	1256	1.16	S10E11	2014/08/01 17:55	2014/08/01 18:13	2014/08/01 18:18	2014/08/01 18:58	W/-/-	0/0/0	0
2014/08/22 11:12	600	993	1.18	N12E01	2014/08/22 10:13	2014/08/22 10:27	…	2014/08/22 10:37	W/-/-	0/-/0	0
2014/08/24 12:36	551	569	0.56	S07E75	2014/08/24 12:00	2014/08/24 12:17	2014/08/24 12:14	…	-/-/-	0/-/0	0
2014/08/25 15:36	555	697	0.46	N05W36	2014/08/25 14:46	2014/08/25 15:11	2014/08/25 15:08	2014/08/25 15:20	W/-/-	0/-/0	0
2014/09/09 00:06	920	1080	0.33	N12E29	2014/09/08 23:34	2014/09/09 00:29	…	2014/09/09 00:05	W/-/-	0/0/0	0
2014/09/10 18:00	1267	1652	1.15	N14E02	2014/09/10 17:21	2014/09/10 17:45	…	2014/09/10 17:45	W/-/-	1/-/0	1
2014/12/17 05:00	587	855	0.46	S20E09	2014/12/17 04:20	2014/12/17 04:51	2014/12/17 04:44	2014/12/17 05:00	W/-/-	0/-/-	0
2014/12/19 01:04	1195	1513	1.48	S11E15	2014/12/18 21:41	2014/12/18 21:58	2014/12/18 22:22	2014/12/18 22:31	W/-/-	0/-/-	0
2014/12/21 12:12	669	906	0.28	S14W25	2014/12/21 11:24	2014/12/21 12:17	…	2014/12/21 12:05	W/-/-	0/-/-	0
2015/02/09 23:24	1106	1148	0.53	N12E61	2015/02/09 22:59	2015/02/09 23:35	2015/02/09 23:14	…	-/-/-	0/-/-	0
2015/03/07 22:12	1261	1304	0.59	S19E74	2015/03/07 21:45	2015/03/07 22:22	2015/03/07 21:57	…	-/-/-	0/-/-	0
2015/03/10 00:00	995	1081	0.75	S18E45	2015/03/09 23:29	2015/03/09 23:53	2015/03/10 00:05	2015/03/10 00:10	W/-/-	0/-/-	0
2015/03/10 03:36	1040	1156	3.85	S15E40	2015/03/10 03:19	2015/03/10 03:24	2015/03/10 03:28	…	-/-/-	0/-/-	0
2015/03/15 01:48	719	932	0.27	S22W25	2015/03/15 01:15	2015/03/15 02:13	2015/03/15 01:27	…	-/-/-	0/-/-	0

Table B1
(Continued)

HCME (UT) (1)	Sky Speed (km s^{-1}) (2)	Space Speed (km s^{-1}) (3)	Acc (km s^{-2}) (4)	Location (5)	Flare Onset (UT) (6)	Flare Peak (UT) (7)	m-Type II (UT) (8)	DH Type II (UT) (9)	WAVES S/C (10)	SEP G/A/B (11)	SGRE (12)
2015/04/23 09:36	857	864	0.29	N12W89	2015/04/23 09:18	2015/04/23 10:07	2015/04/23 09:22	⋯	-/-/-	0/-/-	0
2015/05/05 22:24	715	721	2.00	N15E79	2015/05/05 22:05	2015/05/05 22:11	2015/05/05 22:12	2015/05/05 22:24	W/-/-	0/-/-	0
2015/05/13 18:48	438	730	1.35	N13W16	2015/05/13 18:09	2015/05/13 18:18	2015/05/13 18:21	⋯	-/-/-	0/-/-	0
2015/06/18 17:24	1305	1398	0.35	N15E50	2015/06/18 16:30	2015/06/18 17:36	⋯	2015/06/18 17:42	W/-/-	0/-/-	0
2015/06/21 02:36	1366	1740	0.97	N12E16	2015/06/21 02:06	2015/06/21 02:36	2015/06/21 02:24	2015/06/21 02:33	W/-/-	1/-/-	1
2015/06/22 18:36	1209	1573	0.60	N12W08	2015/06/22 17:39	2015/06/22 18:23	2015/06/22 18:05	2015/06/22 18:20	W/-/-	0/-/-	0
2015/06/25 08:36	1627	1805	2.15	N09W42	2015/06/25 08:02	2015/06/25 08:16	2015/06/25 08:16	2015/06/25 08:35	W/-/-	1/-/-	1
2015/08/22 07:12	547	817	1.36	S15E20	2015/08/22 06:39	2015/08/22 06:49	2015/08/22 06:50	2015/08/22 07:07	W/-/-	0/-/-	0
2015/09/20 18:12	1239	1458	0.78	S22W50	2015/09/20 17:32	2015/09/20 18:03	2015/09/20 18:16	2015/09/20 18:23	W/-/-	0/-/-	0
2015/11/04 14:48	578	987	0.01	N09W04	2015/11/04 14:08	2015/11/05 13:31	2015/11/04 13:43	2015/11/04 14:07	W/-/-	0/-/-	0
2015/12/16 09:36	579	937	0.43	S13W04	2015/12/16 08:27	2015/12/16 09:03	⋯	2015/12/16 08:45	W/-/-	0/-/-	0
2015/12/28 12:12	1212	1471	0.29	S23W11	2015/12/28 11:20	2015/12/28 12:45	⋯	2015/12/28 11:50	W/-/-	0/-/-	0
2016/01/01 23:24	1730	1734	2.22	S25W82	2016/01/01 23:58	2016/01/02 00:11	2016/01/01 23:21	2016/01/02 00:55	W/A/-	1/0/-	0
2016/02/11 21:17	719	1174	0.43	N11W07	2016/02/11 20:18	2016/02/11 21:03	2016/02/11 20:35	⋯	-/-/-	0/0/-	0
2017/04/18 19:48	926	932	0.32	N14E77	2017/04/18 19:21	2017/04/18 20:10	2017/04/18 19:49	⋯	-/-/-	0/1/-	0
2017/07/14 01:25	1200	1422	0.38	S06W29	2017/07/14 01:07	2017/07/14 02:09	⋯	2017/07/14 01:18	W/-/-	1/0/-	0
2017/09/04 20:36	1418	1831	6.10	S10W12	2017/09/04 20:28	2017/09/04 20:33	2017/09/04 20:42	2017/09/04 20:27	W/-/-	1/0/-	0
2017/09/06 12:24	1571	1819	3.37	S08W33	2017/09/06 11:53	2017/09/06 12:02	2017/09/06 12:02	2017/09/06 12:05	W/A/-	1/0/-	1
2017/09/10 16:00	3163	3163	1.70	S09W92	2017/09/10 15:35	2017/09/10 16:06	2017/09/10 16:08	2017/09/10 16:02	W/A/-	1/1/-	1

Note. The SEP column gives major SEP events observed by GOES and the SGRE column gamma-ray flares with a "Delayed" component observed by Fermi/LAT (Ajello et al. 2021).

ORCID iDs

Pertti Mäkelä https://orcid.org/0000-0002-8182-4559
Nat Gopalswamy https://orcid.org/0000-0001-5894-9954
Sachiko Akiyama https://orcid.org/0000-0002-7281-1166
Hong Xie https://orcid.org/0000-0002-0058-1162
Seiji Yashiro https://orcid.org/0000-0002-6965-3785

References

Ackermann, M., Ajello, M., Albert, A., et al. 2014, ApJ, 787, 15
Ackermann, M., Allafort, A., Baldini, L., et al. 2017, ApJ, 835, 219
Afanasiev, A., Aran, A., Vainio, R., et al. 2018, in Solar Particle Radiation Storms Forecasting and Analysis, ed. O. E. Malandraki & N. B. Crosby, Vol. 444 (Berlin: Springer), 157
Ajello, M., Albert, A., Allafort, A., et al. 2014, ApJ, 789, 20
Ajello, M., Baldini, L., Bastieri, D., et al. 2021, ApJS, 252, 13
Akimov, V. V., Afanassyey, V. G., Belaousov, A. S., et al. 1991, ICRC (Dublin), 73
Akimov, V. V., Ambrož, P., Belov, A. V., et al. 1996, SoPh, 166, 107
Allafort, A. J. 2018, PhD thesis, Stanford Univ.
Atwood, W. B., Abdo, A. A., Ackermann, M., et al. 2009, ApJ, 697, 1071
Bougeret, J. L., Goetz, K., Kaiser, M. L., et al. 2008, SSRv, 136, 487
Bougeret, J. L., Kaiser, M. L., Kellogg, P. J., et al. 1995, SSRv, 71, 231
Brueckner, G. E., Howard, R. A., Koomen, M. J., et al. 1995, SoPh, 162, 357
Bruno, A., Bazilevskaya, G. A., Boezio, M., et al. 2018, ApJ, 862, 97
Cheng, X., Zhang, J., Ding, M. D., et al. 2013, ApJL, 769, L25
Chintzoglou, G., Patsourakos, S., & Vourlidas, A. 2015, ApJ, 809, 34
Cliver, E. W., Kahler, S. W., & Reames, D. V. 2004, ApJ, 605, 902
Cliver, E. W., Kahler, S. W., & Vestrand, W. T. 1993, ICRC (Alberta), 91
de Nolfo, G. A., Bruno, A., Ryan, J. M., et al. 2019, ApJ, 879, 90
Domingo, V., Fleck, B., & Poland, A. I. 1995, SoPh, 162, 1
Driesman, A., Hynes, S., & Cancro, G. 2008, SSRv, 136, 17
Eyles, C. J., Harrison, R. A., Davis, C. J., et al. 2009, SoPh, 254, 387
Forrest, D. J., Vestrand, W. T., Chupp, E. L., et al. 1985, ICRC (San Diego, CA), 146
Gopalswamy, N. 2020, Atoms, 8, 14
Gopalswamy, N., & Mäkelä, P. 2014, in ASP Conf. Ser. 484, Outstanding Problems in Heliophysics: From Coronal Heating to the Edge of the Heliosphere, ed. Q. Hu & G. P. Zank (San Francisco, CA: ASP), 63
Gopalswamy, N., Mäkelä, P., Akiyama, S., et al. 2022a, CEAB, 46, 1
Gopalswamy, N., Mäkelä, P., & Yashiro, S. 2022b, in 18th Annual Meeting of the Asia Oceania Geosciences Society, ed. V.-T.-V. Nguyen, S.-Y. Liong, & M. Satoh (Singapore: World Scientific), 189
Gopalswamy, N., Mäkelä, P., Yashiro, S., et al. 2017, JPhCS, 900, 012009
Gopalswamy, N., Mäkelä, P., Yashiro, S., et al. 2018, ApJL, 868, L19
Gopalswamy, N., Mäkelä, P., Yashiro, S., et al. 2019, JPhCS, 1332, 012004
Gopalswamy, N., Mäkelä, P., Yashiro, S., et al. 2020, SoPh, 295, 18
Gopalswamy, N., Yashiro, S., Mäkelä, P., Xie, H., & Akiyama, S. 2021, ApJ, 915, 82
Gopalswamy, N., Xie, H., Akiyama, S., et al. 2013, ApJL, 765, L30
Gopalswamy, N., Xie, H., Akiyama, S., Mäkelä, P. A., & Yashiro, S. 2014, EP&S, 66, 104
Gopalswamy, N., Xie, H., Yashiro, S., et al. 2012, SSRv, 171, 23
Gopalswamy, N., Yashiro, S., Michałek, G., et al. 2002, ApJL, 572, L103
Gopalswamy, N., Yashiro, S., Thakur, N., et al. 2016, ApJ, 833, 216
Howard, R. A., Moses, J. D., Vourlidas, A., et al. 2008, SSRv, 136, 67
Howard, T. A., & Tappin, S. J. 2009, SSRv, 147, 31
Hudson, H. S. 2018, in IAU Symp. 335, Space Weather of the Heliosphere: Processes and Forecasts, ed. C. Foullon & O. E. Malandraki (Cambridge: Cambridge Univ. Press), 49
Hutchinson, A., Dalla, S., Laitinen, T., et al. 2022, A&A, 658, A23
Jin, M., Petrosian, V., Liu, W., et al. 2018, ApJ, 867, 122
Joshi, N. C., Uddin, W., Srivastava, A. K., et al. 2013, AdSpR, 52, 1
Kafexhiu, E., Romoli, C., Taylor, A. M., & Aharonian, F. 2018, ApJ, 864, 148
Kanbach, G., Bertsch, D. L., Fichtel, C. E., et al. 1993, A&AS, 97, 349
Kocharov, L. G., Kovaltsov, G. A., Kocharov, G. E., et al. 1994, SoPh, 150, 267
Kouloumvakos, A., Rouillard, A. P., Share, G. H., et al. 2020, ApJ, 893, 76
Kuznetsov, S. N., Kurt, V. G., Yushkov, B. Y., et al. 2014, in The Coronas-F Space Mission, ed. V. Kuznetsov, Vol. 400 (Berlin: Springer), 301
Lau, Y.-T., Northrop, T. G., & Finn, J. M. 1993, ApJ, 414, 908
Leblanc, Y., Dulk, G. A., & Bougeret, J.-L. 1998, SoPh, 183, 165
Lengyel-Frey, D., Stone, R. G., & Bougeret, J. L. 1985, A&A, 151, 215
Li, L. P., & Zhang, J. 2013, A&A, 552, L11
Mäkelä, P., Gopalswamy, N., & Akiyama, S. 2018, ApJ, 867, 40
Mäkelä, P., Gopalswamy, N., Akiyama, S., Xie, H., & Yashiro, S. 2015, ApJ, 806, 13
Mäkelä, P., Gopalswamy, N., Xie, H., et al. 2019, SunGe, 14, 123
Meegan, C., Lichti, G., Bhat, P. N., et al. 2009, ApJ, 702, 791
Murphy, R. J., Dermer, C. D., & Ramaty, R. 1987, ApJS, 63, 721
Odstrcil, D., & Pizzo, V. J. 2009, SoPh, 259, 297
Patsourakos, S., Georgoulis, M. K., Vourlidas, A., et al. 2016, ApJ, 817, 14
Pesce-Rollins, M., Omodei, N., Krucker, S., et al. 2022, ApJ, 929, 172
Pesce-Rollins, M., Omodei, N., Petrosian, V., et al. 2015, ApJL, 805, L15
Plotnikov, I., Rouillard, A. P., & Share, G. H. 2017, A&A, 608, A43
Ramaty, R., Murphy, R. J., & Dermer, C. D. 1987, ApJL, 316, L41
Ryan, J. M. 2000, SSRv, 93, 581
Ryan, J. M., & Lee, M. A. 1991, ApJ, 368, 316
Scott, C. J., Owens, M. J., de Koning, C. A., et al. 2019, SpWea, 17, 539
Share, G. H., Murphy, R. J., White, S. M., et al. 2018, ApJ, 869, 182
Soni, S. L., Selvakumaran, R., & Thampi, R. S. 2023, FrASS, 9, 1049906
Thernisien, A. 2011, ApJS, 194, 33
Thernisien, A., Vourlidas, A., & Howard, R. A. 2009, SoPh, 256, 111
Vestrand, W. T., & Forrest, D. J. 1993, ApJL, 409, L69
von Rosenvinge, T. T., Reames, D. V., Baker, R., et al. 2008, SSRv, 136, 391
Winter, L. M., Bernstein, V., Omodei, N., & Pesce-Rollins, M. 2018, ApJ, 864, 39
Xie, H., Ofman, L., & Lawrence, G. 2004, JGRA, 109, A03109
Xiong, M., Davies, J. A., Bisi, M. M., et al. 2013, SoPh, 285, 369
Zhang, J., & Dere, K. P. 2006, ApJ, 649, 1100